ELSEVIER

Thermochimica Acta 317 (1998) 117–131

thermochimica acta

Improvement of AC calorimetry for simultaneous measurements of heat capacity and thermal conductivity of polymers

A.A. Minakov[a], Yu.V. Bugoslavsky[a], C. Schick[b,*]

[a]*General Physics Institute, R.A.S., Vavilov st. 38, 117942 Moscow, Russia*
[b]*Department of Physics, University of Rostock, Universitätsplatz 3, 18051 Rostock, Germany*

Received 30 April 1998; received in revised form 18 May 1998; accepted 22 May 1998

Abstract

The method of Temperature Waves Transmission Spectroscopy is developed on the basis of the classical AC calorimetry technique. The idea of the method is to use the information about the phase and amplitude of the temperature wave transmitted through a plate-like sample for simultaneous determination of the sample's heat capacity and thermal conductivity. For the correct application of the method in an experimental set up, it was necessary to study the problem of plane temperature wave transmission through a plate-like multilayered system. This problem was solved analytically for a wide range of experimental conditions. It was shown that the AC calorimeter can be used at relatively high frequencies, when the temperature oscillations in the sample are not quasi-static. Therefore, the width of the appropriate frequency range of classical AC calorimetry can be enlarged. This is of great importance for the applicability of classical AC calorimetry for low heat-conductive materials, such as polymers. It is shown that the dynamic heat capacity and thermal conductivity of polymers can be measured in real time and in a broad frequency region. The method was applied for polystyrene near glass transition and for 4.4′-*n*-octyloxycyanobiphenyl (8OCB) liquid crystal in melting region, smectic–nematic and nematic–isotropic transitions. The possibility of dynamic heat capacity measurements is demonstrated. © 1998 Elsevier Science B.V.

Keywords: AC calorimetry; Dynamic heat capacity; Thermal conductivity; Glass transitions; Phase transitions

1. Introduction

Investigation of relaxation phenomena and phase transitions in polymers is important for understanding their physics, as well as for providing practically valuable information on these materials. In this paper, we show that advanced AC calorimetry can be successfully applied for studying polymers.

AC calorimetry is a powerful technique, which was used for decades for measurements of heat capacity of microsamples [1–6]. The principle is based on the excitation of temperature oscillations in a sample. An oscillating heat flow is supplied to one side of the sample, and the amplitude of temperature oscillations is measured on the other side. This is a key difference of AC calorimetry from other modulation techniques, such as temperature-modulated differential scanning calorimetry (TMDSC) [7]. In the latter case, the measurements are on the very surface where the heat is supplied. Classical AC calorimetry is restricted to quasi-static and quasi-adiabatic conditions, i.e. homogeneous oscillations in the sample, and negligible oscillating heat leakage from the sample. Under these

*Corresponding author. Tel.: +49 381 4981644; fax: +49 381 4981626; e-mail: christoph.schick@physik.uni-rostock.de

PII S0040-6031(98)00380-3

conditions, the amplitude of temperature modulation is inversely proportional to the sample heat capacity. To fulfill these conditions, the measurements need to be carried out in a definite frequency range, which is dependent on experimental parameters, and on sample properties. As was shown in [8], at cryogenic temperatures, the appropriate frequency range can be as large as 1 Hz<f<1000 Hz. However, in many practically important cases, the frequency range tends to zero, or the upper and lower limits can even overlap. In particular, this applies to polymers at room temperatures. This explains the motivation for exploring potentialities of the AC technique beyond the classical restrictions.

In principle, the heat capacity can be measured at frequencies below the lower classical limit, if the heat leaks are carefully calibrated at all frequencies and temperatures of interest, provided the experimental conditions are highly reproducible. Such a detailed and very precise calibration of AC calorimeter was recently performed by Ema and Yao [9], which allowed them to go down to millihertz frequency range. Measurements of polymers at frequencies above the upper limit are also important for dynamic heat capacity investigations.

The focus of this paper is to further advance the AC technique to higher frequencies. We aim to show the unrivalled new capabilities of the AC calorimeter when working at frequencies above the classical limit. In this regime, new information on the sample properties can be obtained by measuring the phase of temperature oscillations. Decreasing the sample's thermal conductivity, κ_s, brings up continuous phase lagging of the measured temperature oscillations (these are measured on the opposite surface with respect to the heated surface). Unlike TMDSC, where the measured phase shift due to the thermal length of the sample is limited within the interval $(0,\pi/4)$, in the AC calorimeter there is no limit on the phase lag. This increases the dynamic range and sensitivity to changes in κ_s. Of course, at large values of the phase lag, the relation between the measured modulation amplitude and the sample heat capacity C_s is no longer simple inverse proportionality. However, the two parameters, C_s and κ_s, can be determined from the two measured values, the amplitude and phase of temperature oscillations. The mathematical algorithm to do so is presented in the first part of the paper.

Next, we compare the principles of AC and TMDSC techniques, and consider what is measured by the AC calorimeter in the case of irreversible or slow-relaxing processes in a sample. We prove that the contribution from the imaginary part of the heat capacity to the measured phase shift has an opposite sign to the contribution of apparatus effects and the finite sample's thermal conductivity. This unique property of AC calorimetry makes it highly relevant to studies of complex systems with a broad range of relaxation times, as well as for studies of phase transitions. Further, we present experimental data obtained on different samples in order to illustrate the capabilities of the developed technique.

Improvement of AC calorimetry has brought up a novel method. Its physical mechanism is transmission of temperature waves through a sample. It can be therefore named *Temperature Waves Transmission Spectroscopy*. When applied to studies of polymers, this method allows obtaining of important information, otherwise not accessible.

2. Plane temperature waves in a multilayered system

Consider a multilayered system, which is heated by an uniform heat flow of oscillating rate $P=P_0\cdot\cos(\omega t)$. The flow is applied to the face of the first layer at $z=0$ and propagates through the layered system along z axis. The cross area S of the system is independent on z. Provided that the heat leakage through the perimeter of the system is negligible, the plane temperature waves $T = Re[T_0 \cdot \exp(i\omega t \pm \boldsymbol{k}z)]$ can propagate across the system, where $\boldsymbol{k} = (i\omega c/\kappa)^{-1/2}$. The damping coefficient of this wave equals $Re(\boldsymbol{k}) = k/\sqrt{2}$ and the wave number equals $\mathrm{Im}(\boldsymbol{k}) = k/\sqrt{2}$, where $k = \mathrm{mod}(\boldsymbol{k})$. The stationary oscillating solution of the heat transfer equation without heat sources can be written in the form of a standing wave: $Re\,\{\exp(i\omega t)\cdot[\boldsymbol{a}(\sinh(\boldsymbol{k}z) + \boldsymbol{b}\cdot\cosh(\boldsymbol{k}z)]\}$. Therefore the standing temperature wave $\boldsymbol{T}_i(z) = \exp(i\omega t)\{\boldsymbol{a}_i\cdot\sinh[\boldsymbol{k}_i(z-\xi_i)] + \boldsymbol{b}_i\cdot\cosh[\boldsymbol{k}_i(z-\xi_i)]\}$ is excited in ith layer, where ξ_i is the coordinate of ith boundary. The complex coefficients $\boldsymbol{a}_i$ and $\boldsymbol{b}_i$ are determined by the boundary conditions for temperature and heat flow amplitudes on the face of the ith layer. Provided that there is no heat leakage from the first (at $z=0$) and from

the last (at $z = \xi_{n+1}$) faces of the system, the boundary conditions yield to the following system of linear equations:

$$\mathbf{M} \times [\boldsymbol{a}_i, \boldsymbol{b}_i, \ldots, \boldsymbol{a}_n, \boldsymbol{b}_n]^T = [\boldsymbol{p}, 0 \ldots, 0]^T, \qquad (1)$$

with the matrix

$$\mathbf{M} = \begin{vmatrix}
-1 & 0 & 0 & 0 & 0 & 0 & \ldots & 0 & 0 & 0 & 0 \\
\mathrm{sh}_1 & \mathrm{ch}_1 & 0 & -1 & 0 & 0 & \ldots & 0 & 0 & 0 & 0 \\
\mathrm{ch}_1 & \mathrm{sh}_1 & -\beta_{21} & 0 & 0 & 0 & \ldots & 0 & 0 & 0 & 0 \\
0 & 0 & \mathrm{sh}_2 & \mathrm{ch}_2 & 0 & -1 & \ldots & 0 & 0 & 0 & 0 \\
0 & 0 & \mathrm{ch}_2 & \mathrm{sh}_2 & -\beta_{32} & 0 & \ldots & 0 & 0 & 0 & 0 \\
0 & 0 & 0 & 0 & \mathrm{sh}_3 & \mathrm{ch}_3 & \ldots & 0 & 0 & 0 & 0 \\
0 & 0 & 0 & 0 & \mathrm{ch}_3 & \mathrm{sh}_3 & \ldots & 0 & 0 & 0 & 0 \\
\ldots & \ldots & \ldots & \ldots & \ldots & \ldots & \ldots & \ldots & \ldots & \ldots & \ldots \\
0 & 0 & 0 & 0 & 0 & 0 & \ldots & \mathrm{sh}_{n-1} & \mathrm{ch}_{n-1} & 0 & -1 \\
0 & 0 & 0 & 0 & 0 & 0 & \ldots & \mathrm{sh}_{n-1} & \mathrm{ch}_{n-1} & -\beta_{n(n-1)} & 0 \\
0 & 0 & 0 & 0 & 0 & 0 & \ldots & 0 & 0 & \mathrm{ch}_n & \mathrm{sh}_n
\end{vmatrix},$$

where $\boldsymbol{p} = P_0/(\kappa_1 S \boldsymbol{k}_1)$, $\mathrm{sh}_i = \sinh(d_i \boldsymbol{k}_i)$, $\mathrm{ch}_i = \cosh(d_i k_i)$, d_i is the thickness of ith layer and $\beta_{i(i-1)} = \kappa_i k_i / \kappa_{(i-1)} k_{(i-1)}$. Consider the matrix $\mathbf{M}_n$ obtained from $\mathbf{M}$ after substituting of the column $[\boldsymbol{p}, 0 \ldots, 0]^{\mathrm{T}}$ in place of the last column in $\mathbf{M}$. The determinant of each of the 2×2 blocks under the matrix diagonal is equal to -1. It can be shown that $\det \mathbf{M_n} = (-1)^n \cdot \boldsymbol{p} \cdot \cosh(d_n \boldsymbol{k}_n)$. Therefore the complex amplitude $\boldsymbol{b}_n$ of the temperature oscillations on the boundary at $z = \xi_n$ between the $(n-1)$th and the nth layers equals:

$$\boldsymbol{b}_n = (-1)^n \cdot \boldsymbol{p} \cdot \cosh(\alpha_n)/\det \mathbf{M}, \qquad (2)$$

where $\alpha_i = d_i \cdot (i\omega c_i/\kappa_i)^{1/2}$. Then $\det \mathbf{M}$ can be presented as follows:

$$\det \mathbf{M} = \underline{(-1)^n \cdot (\kappa_1 \boldsymbol{k} 1)^{-1} \cdot \cosh(\alpha_1)} \ldots \cosh(\alpha_n) \cdot [\boldsymbol{B} + \sum (\kappa_i \boldsymbol{k}_i) \cdot \mathrm{th}(\alpha_i)], \qquad (3)$$

where the sum over i is from 1 to n. The cross terms are presented by the sum $\boldsymbol{B} = \boldsymbol{B}_3 + \boldsymbol{B}_5 + \ldots + \boldsymbol{B}_{2m+1}$, where $2m + 1 \leq n$,

$$\boldsymbol{B}_3 = \sum (\kappa_a \boldsymbol{k}_a) \cdot \beta_{cb} \cdot \mathrm{th}(\alpha_a) \cdot \mathrm{th}(\alpha_b) \cdot \mathrm{th}(\alpha_c),$$

$$B_5 = \sum (\kappa_a \boldsymbol{k}_a) \cdot \beta_{cb} \cdot \beta_{ed} \cdot \mathrm{th}(\alpha_a) \cdot \mathrm{th}(\alpha_b) \cdot \mathrm{th}(\alpha_c) \cdot \mathrm{th}(\alpha_d) \cdot \mathrm{th}(\alpha_e), \qquad (4)$$

and so on for all indexes, such as $a<b<c<d<e\ldots$. The sum $\boldsymbol{B}_3$ is taken over all combinations of three elements from n, $\boldsymbol{B}_5$ – over all combinations of five elements from n, and so on. The cross terms are negligibly small at sufficiently low frequencies. Indeed, $\mathrm{th}(\alpha_i) \approx \alpha_i$ at small α_i, and α_i decreases with frequency as $\alpha_i \sim \sqrt{\omega}$.

In classical AC calorimetry one measures effective heat capacity

$$\boldsymbol{C}_{\mathrm{eff}} = P_0/(i\omega \boldsymbol{T}_A), \qquad (5)$$

which is inversely proportional to the measured complex amplitude $\boldsymbol{T}_{\mathrm{A}}$ (in the adopted notations $\boldsymbol{T}_{\mathrm{A}} = \boldsymbol{b}_n$ – the amplitude at the sample face far from the heater). Suppose the relatively small heat leakage from the system to a thermostat through exchange gas can be described by the only relaxation term, as was shown in [9]. Note that $(S/i\omega)(\kappa_i \boldsymbol{k}_i) = C_i/\alpha_i$. Then, as it follows from Eqs. (2), (3) and (5) that the measured effective heat capacity can be presented as:

$$\boldsymbol{C}_{\mathrm{eff}} = \mathrm{ch}(\alpha_1) \ldots \mathrm{ch}(\alpha_{n-1}) \cdot \exp(-i\pi/4) \cdot [C_1 \cdot \mathrm{th}(\alpha_1)/\alpha_1 + \ldots + C_n \cdot \mathrm{th}(\alpha_n)/\alpha_n + C_{\mathrm{tot}}/i\omega\tau_{\mathrm{R}} + \boldsymbol{B}] \cdot \boldsymbol{F}, \qquad (6)$$

where $\alpha_i = \mathrm{mod}(\alpha_i)$, C_{tot} is the total heat capacity of the system, τ_{R} – relaxation time of the system to the thermal equilibrium with the thermostat, $\boldsymbol{F}$-coefficient depending on the heat leakage into the wires of the thermocouple. As was shown in [8,10] this coefficient can be expressed as:

$$\boldsymbol{F} = 1 + Y \cdot \alpha_w \kappa_w / \kappa_{n-1}, \qquad (7)$$

where Y – geometrical form factor ($\mathrm{mod}(Y) \approx 1$),

$\alpha_w = d_w(\omega c_w/\kappa_w)^{1/2}$, c_w, κ_w – thermal parameters, and d_w – diameter of the thermocouple wire. At low frequencies $\alpha_w \ll 1$ and $F \approx 1$.

3. Temperature oscillations in the heater–sample–sensor–holder system

Consider the AC calorimeter described in [8]. The calorimeter cell – the system for creation and registration of temperature modulation in a disk-shaped sample – consists of a heater, a sensor, and a holder. The sample is placed between the heater and the sensor substrates. Thin layers of vacuum grease (apiezon) can be used for good heat contact at the sample's faces. The heater and the sensor are formed on the surfaces of polished sapphire disks of 3 mm diameter and of d_0=0.1 mm thickness. The heater is a chromium film ca. 0.1 μm, sputtered on the first sapphire substrate. Copper contact pads are sputtered on the film, and copper wires of 0.05 mm diameter are welded to the pads. The resistance of the film after special thermal treatment is stable for 5 years and equals 100±10 Ohm over the temperature range 4.2–400 K. Therefore, the heat flow rate is constant with the error below 1% during an experiment without special precautions, if a balance resistance of 100 Ohm is connected in series with the heater. The power of the resistive heater equals $P_0{\cdot}(1+\cos\omega t)$, where $\omega/2$ is the angular frequency of the electric current and P_0 is the average power of the heater. To form the sensor, a copper field is sputtered on the second sapphire substrate. The thermocouple (Cu–Cu:Fe) microwires of 0.05 mm diameter are welded to the copper field. The sensitivity of the thermocouple is about 0.01 mV K^{-1} in the range 1–400 K. The sensor is glued on a silk net which serves as a holder. Thus, the system consists of four layers, including the sample. The amplitude of temperature modulation is measured on the surface between the sensor and the holder. According to Eq. (6) the value of the measured $\boldsymbol{C}_{\text{eff}}$ of the heater–sample–sensor–holder system can be expressed as follows:

$$\boldsymbol{C}_{\text{eff}} = \text{ch}(\alpha_0)\cdot\text{ch}(\alpha_s)\cdot\exp(-i\pi/4)\cdot[\boldsymbol{A} + \gamma_s\cdot\text{th}(\alpha_s) + \boldsymbol{B}]\cdot\boldsymbol{F},$$
$$\boldsymbol{A} = C_0\text{th}(\alpha_0)/\alpha_0 + C_h\text{th}(\alpha_h)/\alpha_h + (1-i)\Gamma/f,$$
$$2\boldsymbol{B} = \text{th}(\alpha_0)\cdot\text{th}(\alpha_s)\cdot[(\kappa_h\boldsymbol{k}_h)\cdot(\beta_{0s}+\beta_{s0})\cdot\text{th}(\alpha_h) + (\kappa_0\boldsymbol{k}_0)\cdot(\beta_{0s}-\beta_{s0})\cdot\text{th}(\alpha_{0/2})], \quad (8)$$

where $C_h, \alpha_h, C_s, \alpha_s$ and C_0, α_0 – the corresponding parameters of the holder, sample and two sapphire substrates of the heater and the sensor ($\alpha_0/2 = \alpha_1 = \alpha_3$, $C_0/2 = C_1 = C_3$), Γ – the constant, depending on the heat link between the system and the thermostat, $f = \omega/2\pi$ – the frequency of the temperature modulation, and $\gamma_s = C_s/\alpha_s$. The parameters $\alpha_0, \alpha_h, C_0, C_h, \Gamma$, and $\boldsymbol{F}$ can be determined in advance without a sample. Then the two parameters γ_s and α_s can be calculated from the two measured values, $Re\boldsymbol{C}_{\text{eff}}$ and $\text{Im}\boldsymbol{C}_{\text{eff}}$, using the Eq. (8). Finally, the sample heat capacity and thermal conductivity can be expressed as follows:

$$C_s = \gamma_s\cdot\alpha_s,$$
$$\kappa_s = \omega\cdot d_s\cdot\gamma_s/S\cdot\alpha_s. \quad (9)$$

It is noteworthy that, when the results are presented in this form, the accuracy of the measured sample heat capacity is independent of the errors of the measurements of the sample face area S and thickness d_s. It is especially important when sample dimensions are changed in the experiment due to thermal expansion.

4. Calibration of the calorimeter

As the first step to the Temperature Waves Spectroscopy the low frequency limit can be considered. In the first approximation the cross terms $\boldsymbol{B}$ can be neglected and $\boldsymbol{F} = 1$. Then the frequency-dependent effective heat capacity of the empty cell $\boldsymbol{C}_{\text{emp}}(T,f)$ equals:

$$C_{\text{emp}} = \text{ch}(\alpha_0)\cdot\exp(-i\pi/4)\cdot[C_0\cdot\text{th}(\alpha_0)/\alpha_0 + C_h\cdot\text{th}(\alpha_h)/\alpha_h + (1-i)\Gamma/f]. \quad (10)$$

The values of the frequency-independent parameters $C_0, C_h, \alpha_0/(f)^{1/2}, \alpha_h/(f)^{1/2}$ and Γ/C_0 can be obtained from the frequency dependence of $\boldsymbol{C}_{\text{emp}}$ at any fixed temperature. This is only the parameter Γ that depends on ambient gas pressure. But this dependence is very weak in the pressure range 1–100 Pa. In all measurements the pressure of helium gas was ca.10 Pa.

A set of calorimeter cells was calibrated. For example, consider the frequency dependence of $\boldsymbol{C}_{\text{emp}}$ at

300 K for cell N3. The dependences of mod($\boldsymbol{C}_{\rm emp}$) and phase shift $\varphi = -\mathrm{Arg}(\boldsymbol{C}_{\rm emp})$ between temperature modulations in the heater and the sensor are shown in Fig. 1 (note that the phase shift between the heat flow and the sensor temperature equals $\varphi-\pi/2$). As shown in Fig. 1, the experimental dependence $\boldsymbol{C}_{\rm emp}\,(300\mathrm{K},f)$ is well described by Eq. (10) in the frequency range 0.1–40 Hz. The values of the parameters are as follows: C_0=3.8 mJ K^{-1}, $C_{\rm h}$= 2.6 mJ K^{-1}, $\alpha_0/(2f)^{1/2}$=0.3 s$^{1/2}$, $\alpha_{\rm h}/(2f)^{1/2}$=1.1s$^{1/2}$, Γ/C_0=0.03 s^{-1}.

At higher frequencies heat leakage into thermocouple wires becomes important. This explains the discrepancy between the values of measured and calculated $\boldsymbol{C}_{\rm emp}$ at high frequencies, shown in Fig. 1. In the second approximation, the factor $\boldsymbol{F}(T,f)$ in Eq. (6) needs be taken into account. The temperature variations of the cell parameters are shown in the Table 1, for another cell, N9. It is worth mentioning that the cell-to-cell variation of the parameters is due mainly to the variation of sapphire substrate sizes. Once cell calibration is performed, the calibration table is stored in the computer memory. The software that drives the calorimeter uses this table for calculation of $C_{\rm s}$ and $\kappa_{\rm s}$ from the measured values of φ and $C_{\rm eff}$. Thus, the described algorithm makes it possible to carry out simultaneous measurements of heat capacity and thermal conductivity in real time.

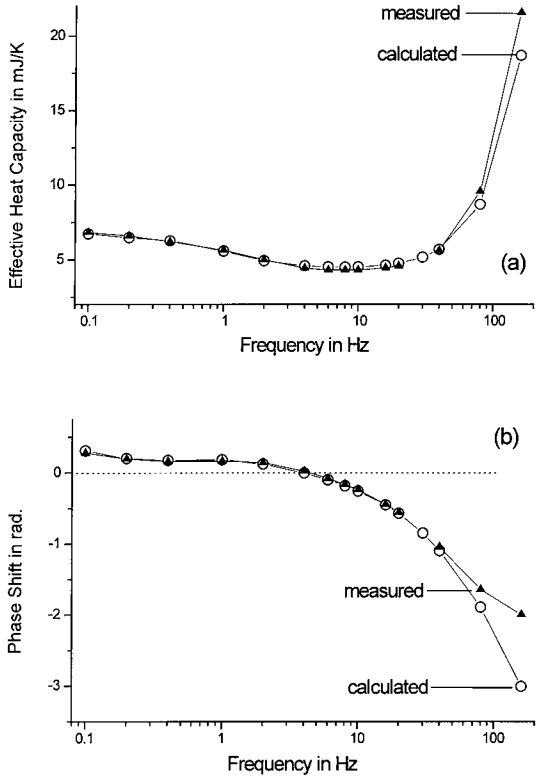

Fig. 1. Frequency dependences of measured (▲) and calculated (○) effective heat capacity $C_{\rm emp}$(300 K) for empty cell; (a) the absolute value of $C_{\rm emp}$ and (b) the phase shift φ=−Arg($C_{\rm emp}$) between temperature modulations in heater and sensor.

Table 1
Thermophysical parameters of the calorimeter cell used in calibration

Temperature/K	Heat capacity/(mJ K^{-1})		$\alpha(2f)^{-1/2}$/(s$^{1/2}$)		(Γ/C_0)/(s^{-1})
	Substrates	Holder	Substrates	Holder	
5.5	5.10E−05	1.20E−03	1.30E−02	8.60E−01	6.20E+01
20	1.00E−02	6.89E−02	2.00E−02	8.70E−01	6.90E+00
50	1.25E−01	2.00E−01	4.50E−02	9.00E−01	4.80E−01
100	9.00E−01	3.00E−01	9.00E−02	1.00E+00	7.00E−02
150	2.15E+00	3.80E−01	1.20E−01	1.00E+00	4.20E−02
200	3.10E+00	8.00E−01	1.65E−01	1.00E+00	3.30E−02
250	4.00E+00	1.20E+00	2.00E−01	1.05E+00	3.00E−02
300	4.70E+00	1.80E+00	2.50E−01	1.10E+00	3.00E−02
350	4.90E+00	2.20E+00	2.80E−01	1.20E+00	3.00E−02
400	5.10E+00	2.60E+00	3.00E−01	1.30E+00	3.00E−02

C_0 Heat capacity of two sapphire substrates of the heater and of the sensor.
α=kd Parameter characterizing the thermal length of a plate of thickness d, where $k = (\omega c/\kappa)^{1/2}$ is the wave number of the temperature wave in this plate at frequency f=$\omega/2\pi$.
Γ/C_0 Parameter of the cell relaxation to the thermal equilibrium with a thermostat.

5. What is measured by the AC calorimeter? Comparison with the TMDSC technique

The complex Fourier transform $\boldsymbol{C}(\omega)$ of the dynamic heat capacity $C(t)$ can be measured by a classical AC calorimeter in the appropriate frequency range. Strictly speaking, the Fourier transform $\boldsymbol{F}[C^{-1}]$ of the inverse dynamic heat capacity $C(t)^{-1}$ is measured. Indeed, the measured value is a complex amplitude $\boldsymbol{T}_{\mathrm{A}}$, which is a response to the applied oscillating heat flow $P(t) = P_0 \cdot \exp(i\omega t)$. The general linear response approximation leads to the following relation:

$$T(t) = \int_0^\infty C^{-1}(\tau) \cdot P(t-\tau)\mathrm{d}_\tau \tag{11}$$

The equation for the Fourier components $\boldsymbol{T}(\omega) = \boldsymbol{F}[C^{-1}] \cdot \boldsymbol{P}(\omega)$ is a consequence of Eq. (11), where the Fourier component of the response function $C^{-1}(t)$ is defined as follows:

$$\boldsymbol{F}[C^{-1}] = \int_0^\infty C^{-1}(t) \cdot \exp(-i\omega t)\mathrm{d}t \tag{12}$$

and $\{\boldsymbol{F}[C^{-1}](\omega)\}^+ = \boldsymbol{F}[C^{-1}](-\omega)\}$.

In the case of time-independent heat capacity $C(t) = C_0$ the Fourier component of the response function is equal to $\boldsymbol{F}[C^{-1}] = 1/(i\omega C_0)$, as it follows from Eq. (12). Of course, this result is in agreement with Eq. (5), i.e. $\boldsymbol{T}_{\mathrm{A}} = P_0/(i\omega C_0)$. In general $\boldsymbol{F}[C^{-1}] = 1/[i\omega \boldsymbol{C}(\omega)]$.

To discuss the case of time-dependent heat capacity, consider the following simple model. Assume that a system consists of two subsystems with fast and slow relaxation. Suppose that C_1, C_2 are heat capacities and τ_1, τ_2 – relaxation times of the fast and slow subsystems respectively, where $\tau_1 \ll \omega^{-1}, \tau_1 \ll \tau_2$ and $C_0 = C_1 + C_2$ is the total heat capacity of the system. Consider variation of the system temperature $T(t)$, when a heat pulse $P_0 \cdot \delta(t)$ is applied to the system ($\delta(t)$ is the delta function). Then the temperature of the system is equal to $T(t) = (P_0/C_0) \cdot [1 + (C_2/C_1) \cdot \exp(-t/\tau_2)] \cdot \theta(t)$, where $\theta(t)$ is the unit step function. The Fourier component of $T(t)$ is equal to $\boldsymbol{T}(\omega) = (P_0/C_0) \cdot [(1/i\omega) + (C_2/C_1)/(i\omega + \tau_2^{-1})]$. Consequently, the Fourier component of the response function $C^{-1}(t)$ can be expressed as follows:

$$\boldsymbol{F}[C^{-1}] = (1/i\omega C_0) \cdot [1 + (C_2/C_1) \cdot (i\omega\tau_2)/(1 + i\omega\tau_2)]. \tag{13}$$

Therefore, the heat capacity becomes complex, when a slow relaxation process occurs in a system.

For measurements of a complex heat capacity it is important to measure $\mathrm{Arg}\{\boldsymbol{F}[C^{-1}]\}$ correctly. The phase shift $\varphi - \pi/2$ between sample temperature and heat flow can be measured by the AC calorimeter. As the trivial phase lag $-\pi/2$ is not of interest, consider the phase shift between the temperature modulations on the opposite sides of a sample. This phase shift is a sum of two contributions. The first contribution is equal to $\mathrm{Arg}\{1/\boldsymbol{C}(\omega)\}$. This contribution to the value of φ is positive. Note, that by definition $\boldsymbol{C}(\omega) = C^{|} - iC^{||}$, where $C^{||} > 0$, as follows from Eqs. (16) and (17) of Section 6. The second contribution is equal to the phase lag φ_{tc}, depending on the system's thermal conductivity. As was shown for a multilayered system in Sections 2–4 the value φ_{tc} depends on parameter $\alpha_{\mathrm{s}}=k_{\mathrm{s}}\mathrm{d}_{\mathrm{s}}$, characterizing the thermal length of the sample. This contribution is negative and it tends to $-\infty$, when the thickness of the sample and/or modulation frequency are increased. Consequently, it is possible to distinguish these two contributions. Therefore, a peak of $\varphi(T)$ dependence, related to $\mathrm{Im}(\boldsymbol{C})$, can be measured. On the other hand, the value of calculated thermal conductivity κ_{s} contains two physically different contributions. The first is true thermal conductivity, related to φ_{tc}. The second is the contribution proportional to $\mathrm{Im}(\boldsymbol{C})$. In this case, calculated thermal conductivity should be renamed *effective thermal conductivity* κ_{eff}, which is equal to the true κ_{s}, when the sample heat capacity is real-valued. Finally, note that the calculated $\boldsymbol{C}_s$ is the absolute value of the complex $\boldsymbol{C}_{\mathrm{s}}$. Of course it is impossible to separate three parameters $\boldsymbol{C}_{\mathrm{s}}$, $\mathrm{Im}\boldsymbol{C}_s$, and κ_s, when only two, T_{A} and φ, are measured. However, in a number of interesting cases (near phase transitions) a maximum proportional to $C^{||}$ can be well defined on top of the background smooth temperature dependence of thermal conductivity, which has no peak, but rather minimum or no anomaly.

On the contrary, in the TMDSC scheme the phases of temperature modulation and heat flow are measured on the same side of the sample. This is the reason why

the two contributions to the phase shift φ are both positive. In this case, the phase shift φ_{tc}, depending on the thermal length of the sample, is positive and changes only from 0 to $\pi/4$, when sample thickness or modulation frequency tends to infinity. Consequently, it is more complicated to distinguish the two mentioned contributions to the phase shift in TMDSC. It is worth noting that it is the transmitted temperature wave that is measured by the AC calorimeter.

6. Phase shift at melting transition

Consider a single heating–cooling cycle, when the sample temperature is arbitrarily changed and returns to its initial value. The total amount of heat absorbed by the sample equals to the integral:

$$Q = \int_{-\infty}^{+\infty} (\mathrm{d}T/\mathrm{d}t) \cdot C(t)\mathrm{d}t \tag{14}$$

This integral can be calculated by analogy to the calculations of electromagnetic field absorption in [11]. In general, the functions $T(t)$ and $C(t)$ can be represented as Fourier integrals and Eq. (14) can be written as follows:

$$Q = \int_{-\infty}^{+\infty}\int_{-\infty}^{+\infty} (1/2\pi)^2 \mathrm{d}\omega'\mathrm{d}\omega \int_{-\infty}^{+\infty} (i\omega) \cdot \boldsymbol{T}(\omega) \cdot \boldsymbol{C}(\omega') \cdot \exp[i(\omega - \omega')t]\mathrm{d}t, \tag{15}$$

where $\boldsymbol{T}(\omega)$ equals to $\boldsymbol{T}(-\omega)$ at even extension of time dependence $T(t)$, i.e. at $T(t) = T(-t)$. As a result of integrating with respect to time, the factor $\delta(\omega - \omega')$ appears in Eq. (15). After integrating with respect to ω', and noting that $\boldsymbol{C}(-\omega) = [\boldsymbol{C}(\omega)]^{+}$, Eq. (15) can be written as

$$Q = (1/2) \int_{-\infty}^{+\infty} (i\omega) \cdot \boldsymbol{T}(\omega).[\boldsymbol{C}(\omega) - (\boldsymbol{C}(\omega))^{+}]\mathrm{d}\omega/2\pi \tag{16}$$

As follows from Eq. (16), $Q \sim i \cdot (\mathrm{Im}[\boldsymbol{C}(\omega)]$. Indeed, the total heat absorbed by the sample is positive in the equilibrium process. Hence, by definition $C^{||} > 0$, provided $\boldsymbol{C}(\omega) = C^{|} - iC^{||}$. Then, Eq. (16) can be written as follows:

$$Q = \int_{-\infty}^{+\infty} \omega \cdot \boldsymbol{T}(\omega) \cdot C''(\omega)\mathrm{d}\omega/2\pi \tag{17}$$

Finally, consider a melting transition with transition enthalpy H, which is uniformly smeared in the temperature interval from T_1 to T_2. Denote the amplitude of the cycle as T_A and $\lambda = H/(T_2 - T_1)$, where $T_A < (T_2 - T_1)$. In the case of completely reversing the melting–crystallization cycle, the heat $Q = \lambda \cdot T_A$, absorbed on heating, is the same as released at cooling. In this case, the excess heat capacity C_{ex} arising due to melting–crystallization, is real-valued and $C_{ex}=\lambda$. The Fourier component of C_{ex} is equal to $\boldsymbol{C}_{ex}(\omega) = \lambda \cdot \delta(\omega)$. If the cycle is non-reversing, a part $\varepsilon \cdot Q$ of the heat absorbed on heating is not released on cooling. In this case, the effective non-zero imaginary contribution $C^{||} \sim \varepsilon\lambda$ to excess heat capacity appears, as it follows from Eq. (17). For harmonic temperature modulation the integral in Eq. (17) is equal to $\omega T_A C^{||}$. Then

$$C''(\omega) = \varepsilon \cdot \lambda/\omega \tag{18}$$

This result is in agreement with the calculations for different models discussed in [12]. Consequently, the Fourier component of the excess heat capacity can be expressed as $\boldsymbol{C}_{ex}(\omega) \approx \lambda \cdot \delta(\omega) + \varepsilon \cdot \lambda/(i\omega)$. Actually, the average value $\langle \boldsymbol{C}_{ex}(\omega) \rangle$ over the frequency interval $(\omega - \Delta\omega/2, \omega - \Delta\omega/2)$ is measured, where $\Delta\omega = 1/\tau_a$ and τ_a is the apparatus time constant. After averaging over this frequency interval we have the measured value of the dynamic excess heat capacity $\langle \boldsymbol{C}_{ex}(\omega) \rangle \approx \lambda + \varepsilon \cdot \lambda/(i\omega\tau_a)$.

Therefore, the excess heat capacity $\boldsymbol{C}_{ex} \approx \lambda + \varepsilon \cdot \lambda/(i\omega\tau_a)$ can be measured by the AC calorimeter in the case of non-reversing cycling at melting transition. The positive phase shift φ should be measured in this case. This shift is opposite to the shift φ_{tc}, which arises due to the lag in the phase depending on the thermal conductivity of the sample.

7. Results and discussion

7.1. Cryogenic measurements

Cryogenic measurements were performed to verify the calculation algorithm and the calibration.

At low temperatures, the thermal conductivity of sapphire is extremely high and the heat capacity of the sapphire substrates is small in comparison to sample heat capacity. This is the reason why at low temperatures the cross terms and heat leakage into the thermocouple can be neglected in a very broad frequency range. As was shown in [8] the upper frequency limit can be as high as 1 kHz. To check the calculation algorithm in a broad range of modulation amplitudes T_A the measurements were performed near the heat capacity peak at a magnetic phase transition. The method was applied to the antiferro-paramagnetic phase transition in monocrystalline $ZnCr_2Se_4$ at Neel temperature $T_N \approx 20.7$ K. In the peak at $T = T_N$ the amplitude T_A was ca.10^{-2} and 10^{-4} K at modulation frequencies 4 and 120 Hz, respectively. On the shoulders of the peak at $T = T_N \pm 1$ K the amplitude T_A varied from 0.04 to 0.001 K, when the frequency was changed from 4 to 120 Hz. The underlying heating–cooling rate q was ca.5 K min^{-1} at temperatures far from the phase transition and ca.0.1 K min^{-1} near the transition. It is worth noting that, when the amplitude T_A is smaller than q/ω, the sample temperature is a monotonic function of time. In the experiment, the amplitude T_A was ca. 10 times larger than q/ω. So the sample temperature oscillated at all these amplitudes and frequencies. The results were the same in the cooling and heating processes. No hysteresis was observed.

The measurements were performed on the plate-like sample of face area 5 mm^2 and of 0.43 mm thickness at the amplitude P_0=0.42 mW. Temperature dependences of the effective heat capacity $C_{\text{eff}} = \text{mod}[P_0/(i\omega \boldsymbol{T}_A)]$ and the phase shift φ are shown in Fig. 2.

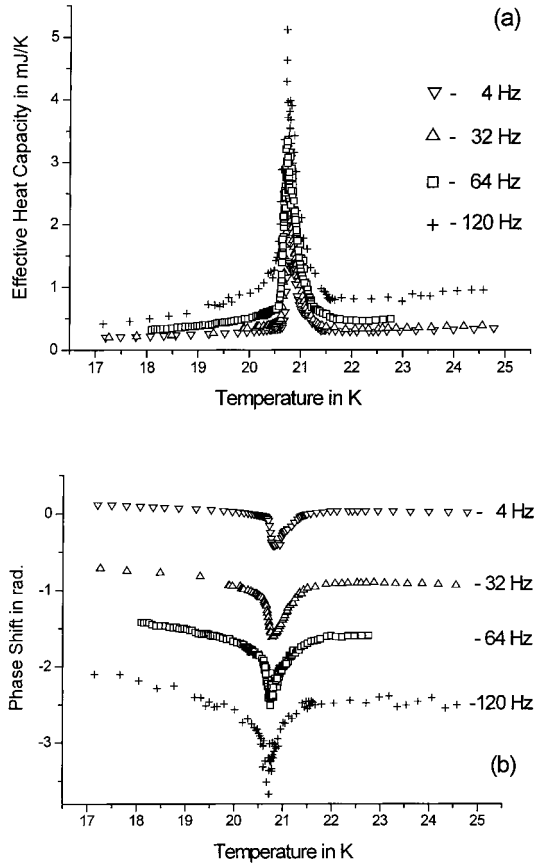

Fig. 2. Temperature dependences of (a) the effective heat capacity and (b) the phase shift near the antiferro-paramagnetic phase transition in monocrystalline $ZnCr_2Se_4$ at different frequencies. The measurements were performed at the amplitude of the heat flow rate P_0= 0.42 mW, underlying cooling–heating rate ca.0.1 K min^{-1} (near the phase transition) and 5 K min^{-1} – far from the phase transition.

As is shown in Fig. 2, the temperature modulation was quasi-static at 4 Hz (the phase shift $\varphi \approx 0$) and this was not quasi-static at higher frequencies (the phase shift (reaches $-\pi$ at 120 Hz). The calculated temperature dependences of the true sample heat capacity C_s and thermal conductivity are shown in Fig. 3. Of course, the sample heat capacity C_s is frequency-independent. It is remarkable that such different curves in Fig. 2 are converted to a single curve in Fig. 3. This result verifies that improved AC calorimetry can be applied at high frequencies when sample temperature modulation is not quasi-static.

Note that in the close vicinity of the Neel point the relaxation time of the magnetic subsystem tends to infinity due to critical slowing down. This is the reason why the magnetic part of the sample heat capacity near phase transition depends on the rate of temperature variation. Consequently, the Fourier transform $\boldsymbol{C}_s(\omega)$ of the sample heat capacity $C_s(t)$ is complex. The imaginary part, $\text{Im}\boldsymbol{C}_s(\omega)$, gives an additional contribution to the phase shift φ. Therefore, the value of κ_s, calculated using the above algorithm contains two physically different contributions: true thermal conductivity and the contribution proportional to $\text{Im}\boldsymbol{C}_s$. Hence, the calculated κ_s should be named as effective thermal conductivity κ_{eff}. Note that the calculated C_s is the absolute value of the complex $\boldsymbol{C}_s$. In Fig. 3 a

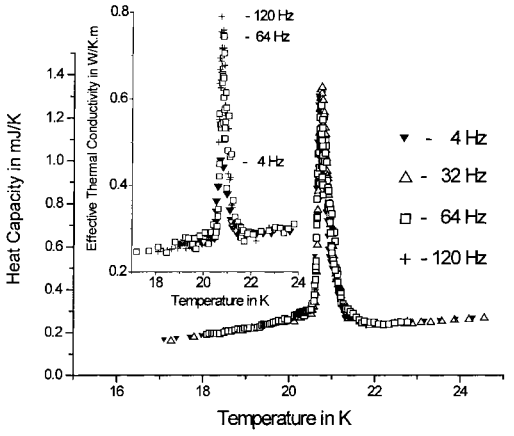

Fig. 3. Heat capacity C_s and the effective thermal conductivity κ_{eff} (in the insert) near phase transition in $ZnCr_2Se_4$ at different frequencies. The conditions are the same as in Fig. 2. The peak of $\kappa_{eff}(T)$ at Neel temperature is due to $\mathrm{Im}C_s$ contribution to the phase shift φ.

maximum proportional to $C^{||}$ is well defined on the top of background smooth temperature dependence of thermal conductivity, which has no peak, but rather minimum or no anomaly. As shown in Fig. 3 the value of the peak of $C^{||}$ at T_N increases with frequency and reaches maximum at ca.10^2 Hz.

7.2. Glass transition in polystyrene

To check the applicability of the developed method to polymer materials, the sample of polystyrene (PS 168 N, BASF) was studied in the glass transition region. At low frequencies (f<1 Hz) the measured heat capacity is in good agreement with the ATHAS data bank available through the World Wide Web on the Internet [14], which again convinced us that the cell calibration is correct. The measurements were performed at underlying heating and cooling rate q ca.5 K min^{-1}, the amplitude of the heat flow rate P_0 was varied in the range 1–40 mW and T_A in the range 1–300 mK at frequencies in the range 0.4–16 Hz. It was found that the heating and cooling curves became reproducible and without hysteresis after one or two heating–cooling cycles. PS has low thermal conductivity, and heat flux through the sample was sufficiently large to produce a noticeable difference of mean temperatures at two sample faces. This temperature difference ΔT_s can be estimated as

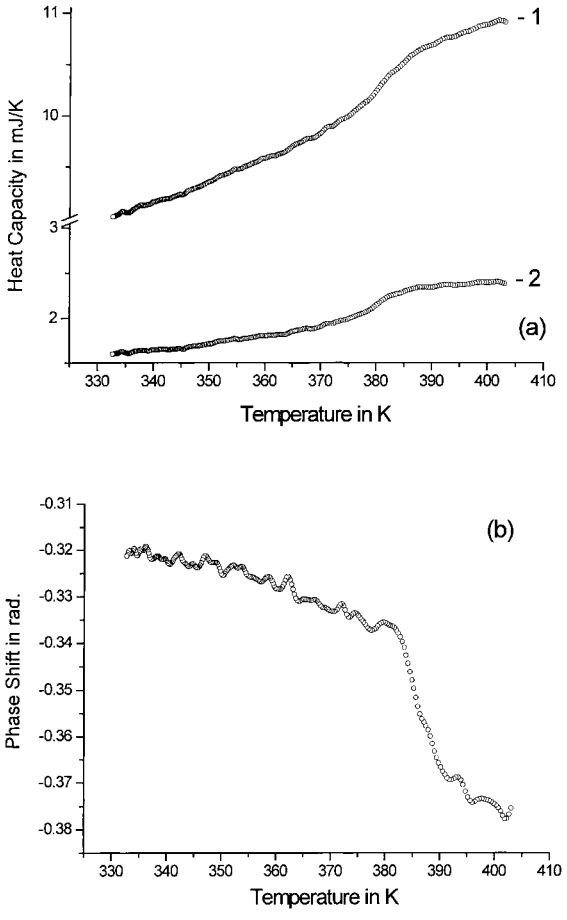

Fig. 4. Glass transition in the polystyrene sample of thickness 0.15 mm at frequency 0.4 Hz, underlying the heating–cooling rate 5 K min^{-1}, the amplitude of the heat flow rate P_0=6.6 mW, modulation amplitude T_A≈0.3 K, and temperature difference across the sample ΔT_s≈0.6 K; (a) the effective heat capacity (1) and the true heat capacity (2); (b) the phase shift φ between temperature modulations in the heater and the sensor.

$\Delta T_s = (P_0 d_s)/(2S\kappa_s)$. Therefore, the average sample temperature equals $T_s = T + \Delta T_s/2$, where T is the temperature measured by the sensor.

The PS sample had a disk shape, with a diameter of 3.2 mm and a thickness of 0.15 mm. Temperature dependences of φ, C_{eff} and C_s at frequency f=0.4 Hz are shown in Fig. 4. These dependences were measured at P_0=6.6 mW, T_A≈0.3 K and $\Delta T_s/2$=0.3 K. The amplitude T_A was 10 times larger than q/ω. Therefore, the sample temperature was an oscillating function of time. The dependences of the effective

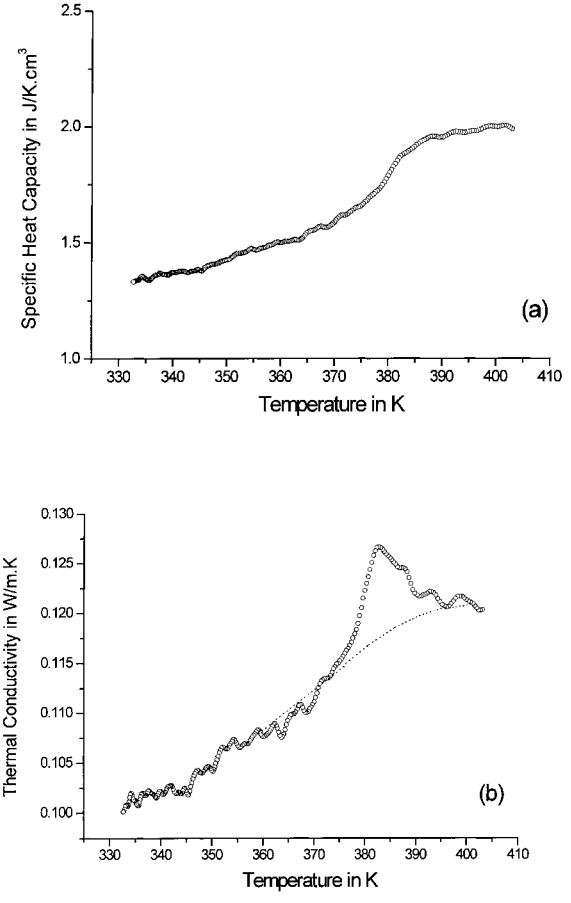

Fig. 5. Glass transition in the polystyrene at the same conditions as in Fig. 4; (a) the specific heat capacity c_s, (b) the effective thermal conductivity κ_{eff}. Dotted line shows (approximately) the true thermal conductivity. The peak of $\kappa_{eff}(T)$ at glass transition temperature is due to ImC_s contribution to the phase shift φ.

thermal conductivity and the specific heat capacity c_s are shown in Fig. 5.

Note that near glass transition temperature T_g the heat capacity of polystyrene is complex [13]. The imaginary part of the heat capacity Im$\boldsymbol{C}_s$ gives an additional contribution to the phase shift φ. Therefore, the calculated effective thermal conductivity κ_{eff} contains the contribution proportional to Im$\boldsymbol{C}_s$.

At frequencies higher than 1 Hz the measured values of heat capacity were larger than true values, and increased with frequency. The same effect was observed on sapphire samples at f>10 Hz. The higher the sample thermal conductivity, the higher the frequency limit of the applicability of these calculations.

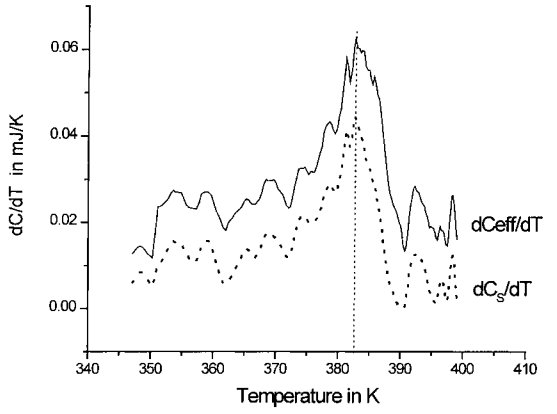

Fig. 6. Temperature dependences of the derivatives dC_{eff}/dT and dC_s/dT at 1 Hz for the same sample as in Fig. 4. Glass transition temperature, as determined from the peak in the derivative C_{eff}/dT is the same as determined by dC_s/dT.

This is due to the effect of cross terms and of the heat leakage into the thermocouple wires. These effects can be taken into account in the second-order approximation. Calibration and software in this approximation are currently in progress.

It was found that the glass transition temperature T_g obtained from the dependence $C_s(T)$ coincides with T_g obtained from $C_{eff}(T)$ as shown in Fig. 6. The dependence $T_g(f)$ derived from $C_{eff}(T,f)$ is shown in Fig. 7. This is in agreement with the results presented in [15].

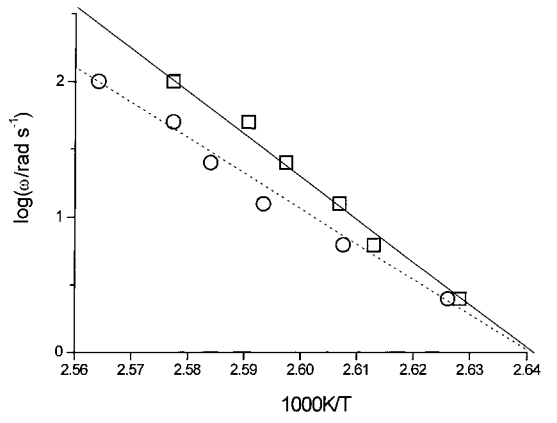

Fig. 7. Activation diagram from the effective heat capacity $C_{eff}(T)$ for polystyrene, where the glass transition temperature is determined by the peak of dC_{eff}/dT (□). The corrected points (○) were obtained after correction by the temperature difference DT_s across the sample.

7.3. Melting and crystallization in water

As was shown in Section 6, the excess heat capacity $\boldsymbol{C}_{ex} \approx \lambda$ can be measured by the AC calorimeter at the melting transition. The positive phase shift φ due to imaginary contribution $\mathrm{Im}(C_{ex}) \approx \varepsilon \cdot \lambda/(i\omega)$ to excess heat capacity should be measured in the case of non-reversing cycling. To verify this experimentally, the dynamic heat capacity of water at melting and crystallization was measured at different amplitudes T_A and modulation frequencies. To avoid any additional phase shift, the measurements were performed without any cuvette. A water drop of volume V ca.10^{-3} cm^3 was placed between the sapphire substrates of the heater and the sensor. The shape of the drop was maintained by surface tension force. The thickness of the layer of water was ca.0.1 mm. The thermal conductivity of water was sufficiently large and the temperature modulation was almost quasi-static. Unfortunately, the drop kept evaporating during the experiment and it was impossible to compare the results at different frequencies quantitatively. However, the results were reproducible during two or three cycles and the results were qualitatively the same for large (ca.$5\cdot10^{-3}$ cm^3) and small (ca.10^{-4} cm^3) drops.

Temperature dependences of the effective heat capacity $C_{eff} = \mathrm{mod}[P_0/(i\omega \boldsymbol{T}_A)]$ and the phase shift φ are shown in Fig. 8.

The measurements were performed for the drop of volume $V\approx7\cdot10^{-4}$ cm^3 and of thickness $d\approx0.1$ mm, at the amplitude P_0=2.3 mW and modulation frequency f=1 Hz. The underlying heating–cooling rate q was ca.5 K min^{-1} at temperatures far from the melting point and ca. 0.3 K min^{-1} near the melting transition. The modulation amplitude T_A was ca. $5\cdot10^{-2}$ K far from the melting point and ca. 10^{-3} K at the melting point. Thus the amplitude T_A was 5 times larger than q/ω far from the melting point, but it was ca. q/ω at the melting point. So the sample temperature was an oscillating function of time except in the close vicinity of the heat capacity peak, when the amplitude T_A was as small as 10^{-3} K. As is shown in Fig. 8, the effective heat capacity is enormously large in melting region at heating and it is normal for water at cooling. So a huge excess heat capacity due to the melting process is observed. However, the most interesting result is the large positive phase shift at heating near the melting point. Note that at heating the phase shift is negative at

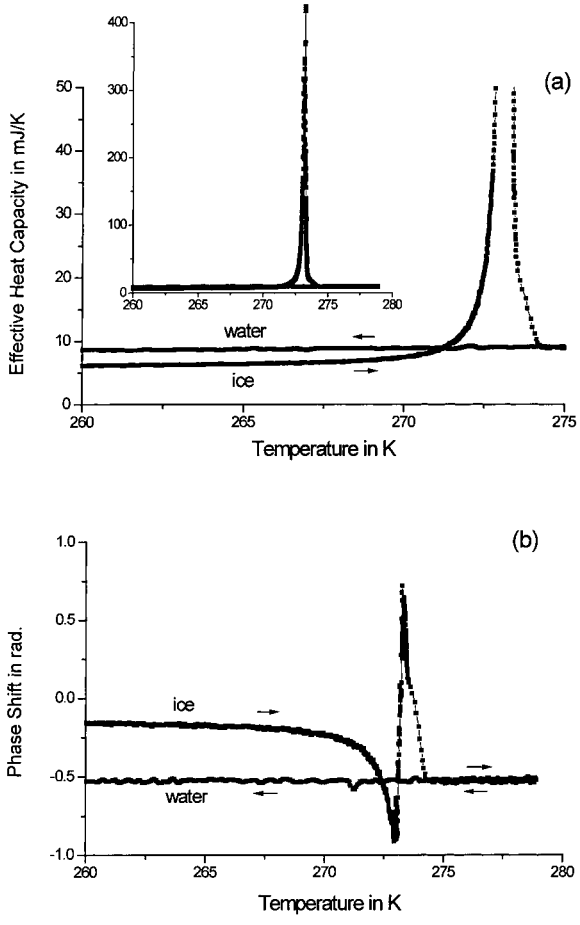

Fig. 8. Temperature dependences of (a) the effective heat capacity and (b) the phase shift for water. The measurements were performed for the water drop of volume $V\approx7\cdot10^{-4}$ cm^3 and of thickness $d\approx0.1$ mm, at frequency f=1 Hz, and the amplitude of the heat flow rate P_0=2.3 mW. The underlying heating–cooling rate was ca.5 K min^{-1} at temperatures far from the melting point and ca.0.3 K min^{-1} near the melting transition. The modulation amplitude T_A was ca. $5\cdot10^{-2}$ K far from the melting point and ca.10^{-3} K at the melting point.

the beginning of the melting process. This negative shift is attributed to the increase of heat capacity and decrease of thermal conductivity when the melting process begins. There is no anomaly at cooling, because the super-cooling water was crystallized only below 260 K. The water was not specially cleaned (only boiled previously), but it was sufficient to observe such a large super-cooling effect. The only reason of this enormous positive phase shift is the

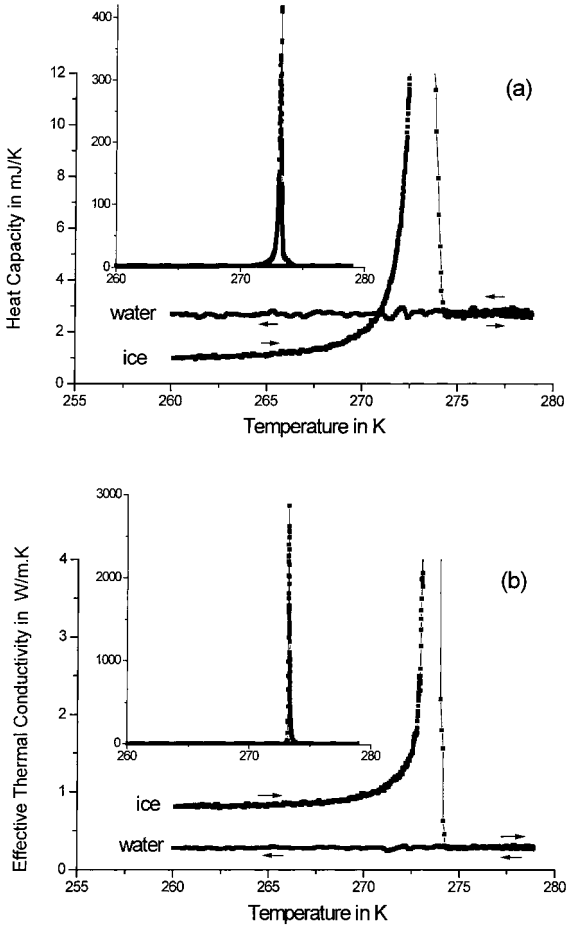

Fig. 9. (a) Heat capacity and (b) effective thermal conductivity of water at the same conditions as in Fig. 8.

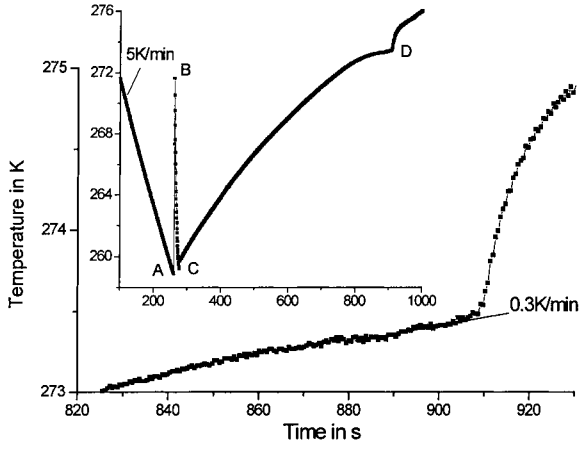

Fig. 10. Time dependence of the sample temperature at the same conditions as in Fig. 8. The crystallization of the supercooling water begins below 260 K (at point A). The crystallization process is accompanied by temperature jump up to the melting point.

contribution to the phase of $\mathrm{Arg}(1/\boldsymbol{C}_{ex})$. This is due to the imaginary part of the excess heat capacity $\mathrm{Im}(\boldsymbol{C}_{ex}) \approx \varepsilon \cdot \lambda/(i\omega)$, as it is shown in Section 6. Any apparatus contribution should be negative! In Fig. 9 the temperature dependences of the true heat capacity and effective thermal conductivity are shown. Time dependence of the sample temperature is shown in Fig. 10. Crystallization of the super-cooling water begins below 260 K (at point A). The crystallization process is accompanied by temperature jump up to the melting point and back to 260 K. This is possible because the fine cell of the calorimeter is placed on the fine silk net. Average sample temperature is controlled by the thermostat via the exchange helium gas. In the melting region the underlying heating rate is very slow (ca.0.3 K min^{-1}) due to irreversible heat absorption at melting. This fact verifies that $\mathrm{Im}(\boldsymbol{C}_{ex})$ should be measured in this region, as follows from Eqs. (17) and (18).

Finally, it is interesting to measure the dynamic excess heat capacity in the non-equilibrium process at crystallization of the super-cooling water. For this purpose, the drop of about 2 times smaller than in the previous experiment was investigated. In this case, the jump of sample temperature was not so large. Therefore, it was possible to measure the temperature dependences of the effective heat capacity C_{eff} and the phase shift φ at crystallization. In Fig. 11 the temperature dependences of C_{eff} and φ are shown. The dependences were measured at the amplitude P_0=6.6 mW and modulation frequency f=2 Hz. The underlying heating–cooling rate was the same as in the previous experiment. Modulation amplitude T_A was ca. 0.1 K far from the melting point and ca. 0.03 K at the melting point. Thus, the amplitude T_A was 10 times larger than q/ω. Therefore, the sample temperature was an oscillating function at all temperatures. The thickness of the water layer was below 0.1 mm. The modulation was quasi-static and the negative phase shift was very small. As is shown in Fig. 11, excess heat capacity is negative at crystallization because heat is released. The phase shift is large and positive. Thus, the value $\mathrm{Im}(\boldsymbol{C}_{ex})$ is also as large at crystal-

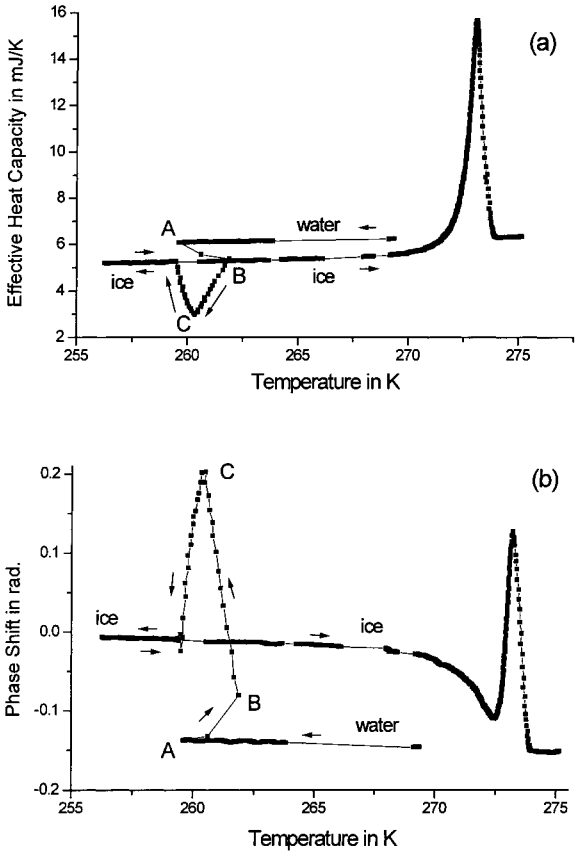

Fig. 11. Temperature dependences of (a) the effective heat capacity and (b) the phase shift for the water drop of volume ca.$4\cdot10^{-4}$ cm^3 and of thickness d<0.1 mm, at frequency f=2 Hz, and the amplitude of the heat flow rate P_0=6.6 mW. The underlying heating–cooling rate was the same as in Fig. 8. The modulation amplitude T_A was ca.0.1 K far from the melting point and ca.0.03 K at the melting point.

lization as at melting, but the excess heat capacity $\boldsymbol{C}_{ex}$ is negative. It is shown qualitatively, that the higher the frequency the smaller the anomaly of the excess heat capacity.

7.4. Phase transitions in the liquid crystal 8OCB

The method was applied to 4.4′-*n*-octyloxycyanobiphenyl (8OCB) liquid crystal in the melting region, smectic–nematic and nematic–isotropic transitions. The measurements were performed at two sample arrangements. First, when the sample was placed between the sapphire substrates of the heater and the sensor without any cuvette. In the liquid state, the sample shape was supported by the surface tension force, as in the experiment with water and second, when a sample was placed in a cuvette with fixed thickness d=0.13 mm. In both cases, the results were the same. Consequently, the thickness of the sample without cuvette did not noticeably change. Therefore, the results without cuvette were reliable. The heating and cooling curves were reproducible after one heating–cooling cycle. Thermal conductivity of this liquid crystal is about five times larger than of polystyrene and the upper frequency limit is also higher. Thus, the calculated C_s and κ_s were independent on frequency up to ca.5 Hz. At higher frequencies this values become larger because of the effect of cross terms and the heat leakage into the thermocouple.

Temperature dependences of C_{eff} and phase shift φ for a plate-like sample of 7 mm^2 face area, of 0.13 mm thickness and at frequency f=4 Hz are shown in Fig. 12. These dependences were measured at P_0=6.6 mW, T_A(340 K)=10 mK and $\Delta T_s/2$=0.06 K. To avoid any additional phase shift, the measurements were performed without any cuvette.

The calculated dependences of thermal conductivity and the sample heat capacity C_s are shown in Fig. 13. It is remarkable that the complicated curves in Fig. 12 are converted to the very simple dependences shown in Fig. 13.

It was found that the thermal conductivity in smectic state was slightly history-dependent, in contrast to the fully reversible behavior in the nematic and isotropic states. The sample heat capacity C_s was history-independent in all these states except in the melting region. The transitions at melting T_m, smectic A-nematic T_{sn}, and nematic–isotropic T_{ni} temperatures were well defined and at the same positions (with an accuracy of ca. 1 K) as has been observed in [16]. A very large contribution of Im$\boldsymbol{C}_s$ to the phase shift was found, in the melting region, when heating. In the melting region the sample heat capacity was complex due to excess heat capacity related to latent heat. The excess heat capacity appeared only in heating curves, when the melting process could be modulated. On the contrary, this contribution fully disappeared in the cooling regime. The maximum of Im$\boldsymbol{C}_s$ in the melting region was well defined on the top of background smooth temperature dependence of $\kappa_s(T)$, which had no anomaly in this region, as shown in the cooling

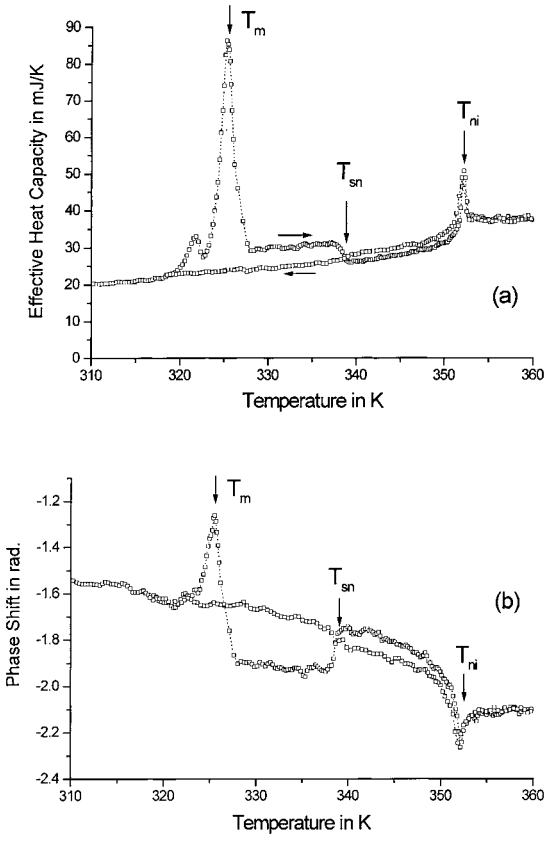

Fig. 12. Temperature dependences of (a) the effective heat capacity and (b) the phase shift for a liquid crystal (8OCB) sample of thickness 0.13 mm at frequency 4 Hz, underlying cooling–heating rate 5 K min^{-1}, the amplitude of the heat flow rate P_0=6.6 mW, modulation amplitude $T_A \approx 0.01$ K, and temperature difference across the sample $\Delta T_s \approx 0.1$ K.

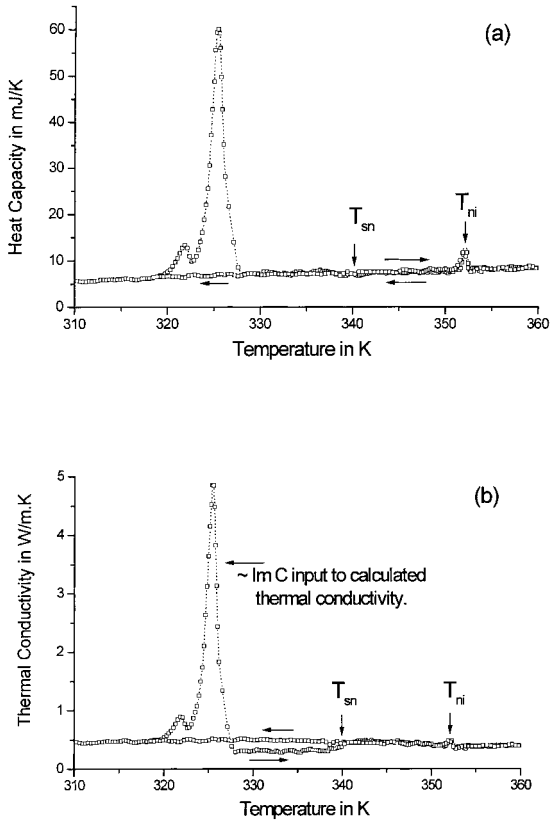

Fig. 13. (a) Heat capacity and (b) the effective thermal conductivity of liquid crystal (8OCB) at the same conditions as in Fig. 12.

curve of Fig. 13. Indeed, due to the super-cooling effect the melting process cannot be modulated. These results illustrate clearly that the information about $\mathrm{Im}\boldsymbol{C}_s$ is contained in the effective thermal conductivity κ_{eff}.

8. Conclusions

The analysis of plane temperature waves transmission through a plate-like multilayered system shows that a classical AC calorimeter can be used for Temperature Waves Transmission Spectroscopy. A method is developed which enables one to use the information about phase and amplitude of the sample temperature modulation for simultaneous measurements of heat capacity and thermal conductivity. Thus, the AC calorimeter can be used at relatively high frequencies, when temperature oscillations in a sample are not quasi-static. Cryogenic experiments show that the measurements can be performed, when temperature oscillations on the opposite faces of a sample are shifted by π and the amplitudes of temperature modulation differ by an order of magnitude. Therefore, the width of an appropriate frequency range of the classical AC calorimetry is enlarged. It is shown that the dynamic heat capacity and thermal conductivity of polymers can be measured in real time and in a broad frequency range. In the same experiment it is shown for polystyrene, that glass transition temperature T_g obtained from true $C_s(T)$ coincides with T_g obtained from C_{eff}, when the product of heat capacity and thermal conductivity is measured. Hence, T_g of PS

measured by 3ω method should coincide with the results from heat capacity measurements. In the melting region near phase and glass transitions the heat capacity is complex. The phase shift φ contains the information about the imaginary part of the complex heat capacity. Therefore, near a phase transition the value of thermal conductivity, calculated from the phase shift, contains the information about $\mathrm{Im}\boldsymbol{C}_s$. Actually, near phase transitions the maximum proportional to $\mathrm{Im}\boldsymbol{C}_s$ is well defined on the top of background temperature dependence of thermal conductivity. A possibility of a reliable separation of $\mathrm{Im}\boldsymbol{C}_s$ contribution from thermal conductivity was demonstrated for water and liquid crystal 8OCB in the melting region.

In conclusion, the improvement of AC calorimetry has brought up a novel method. Its physical mechanism is transmission of temperature waves through a sample. It can therefore be named Temperature Waves Transmission Spectroscopy. When applied to studies of polymers, this method allows to obtain important information, not otherwise accessible.

Acknowledgements

The financial support of the European Commission, grant number IC15CT96-0821, is gratefully acknowledged.

References

[1] P.F. Sullivan, G. Seidel, Phys. Rev. 173 (1968) 679.
[2] P. Handler, D.E. Mapother, M. Rayl, Phys. Rev. Lett. 19 (1967) 356.
[3] M.B. Salamon, Phys. Rev. B 2 (1970) 214.
[4] I. Hatta, A. Ikushima, J. Phys. Chem. Solids 34 (1973) 57.
[5] Y.A. Kraftmakher, Compendium of Thermophysical Property Measurement Methods, vol. 1, Plenum Press, New York, London, 1984, p. 591.
[6] E. Gmelin, Thermochim. Acta 304/305 (1997) 1.
[7] M. Reading, Trends Polym. Sci. 8 (1993) 248.
[8] A.A. Minakov, Thermochim. Acta 304/305 (1997) 165.
[9] K. Ema, H. Yao, Thermochim. Acta 304/305 (1997) 157.
[10] A.A. Minakov, O.V. Ershov, Cryogenics (ICEC Supplement) 34 (1994) 461.
[11] L.D. Landau, E.M. Lifshitz, Electrodynamics of Continuous Matter, Theoretical Physics vol. 8, Moscow, 1982, p. 379.
[12] J.E.K. Schawe, E. Bergmann, Thermochim. Acta 304/305 (1997) 179.
[13] S. Weyer, A. Hensel, C. Schick, Thermochim. Acta 304/305 (1997) 267.
[14] WWW address: http:// funnelweb.utcc.utk.edu/~athas.
[15] S.Weyer, A.Hensel, J.Korus, E.Donth, C.Schick, Thermochim. Acta 304/305 (1997) 251.
[16] A. Hensel, C. Schick, Thermochim. Acta 304/305 (1997) 229.